DAVID, W. I. F. & WOOD, I. G. (1983). *J. Phys. C*, **16**, 5127-5148.
FERGUSON, R. B. (1957). *Can. Mineral.* **6**, 72-77.
FINGER, L. W. & KING, H. E. (1978). *Am. Mineral.* **63**, 337-342.
FINGER, L. W. & PRINCE, E. (1975). *Natl Bur. Stand. (US) Tech. Note* 854.
HAMILTON, W. C. (1974). *International Tables for X-ray Crystallography*, Vol. IV, pp. 273-284. Birmingham: Kynoch Press. (Present distributor D. Reidel, Dordrecht.)
HAZEN, R. M. & FINGER, L. W. (1982). *Comparative Crystal Chemistry*. Chichester: John Wiley.
HAZEN, R. M. & MARIATHASAN, J. W. E. (1982). *Science*, **216**, 991-993.
KING, H. E. & FINGER, L. W. (1979). *J. Appl. Cryst.* **12**, 374-378.
KOMKOV, A. I. (1959). *Kristallografiya*, **4**, 836-841.
PINCZUK, A., WELBER, B. & DACOL, F. H. (1979). *Solid State Commun.* **29**, 515-518.
PRINCE, E. (1982). *Mathematical Techniques in Crystallography and Materials Science*. New York: Springer.
SAMARA, G. A. (1977). *Comments Solid State Phys.* **8**, 13-22.
TAKEI, H. & TSUNEKAWA, S. (1977). *J. Cryst. Growth*, **38**, 55.
TANAKA, M., SAITO, R. & WATANABE, D. (1980). *Acta Cryst.* A**36**, 350-352.
TSUNEKAWA, S. & TAKEI, H. (1978). *Phys. Status Solidi A*, **50**, 695-702.
WOOD, I. G., WELBER, B., DAVID, W. I. F. & GLAZER, A. M. (1980). *J. Appl. Cryst.* **13**, 224-229.

Acta Cryst. (1985). B**41**, 184-190

Electron Density in Non-Ideal Metal Complexes. I. Copper Sulphate Pentahydrate

BY J. N. VARGHESE AND E. N. MASLEN*

Crystallography Centre, University of Western Australia, Nedlands, Western Australia 6009, *Australia*

(*Received* 11 *October* 1983; *accepted* 14 *December* 1984)

Abstract

The structure of copper sulphate pentahydrate was refined using an accurate set of X-ray data: $M_r = 249{\cdot}68$, triclinic, $P\bar{1}$, $a = 6{\cdot}1224\ (4)$, $b = 10{\cdot}7223\ (4)$, $c = 5{\cdot}9681\ (4)$ Å, $\alpha = 82{\cdot}35\ (2)$, $\beta = 107{\cdot}33\ (2)$, $\gamma = 102{\cdot}60\ (4)°$, $V = 364{\cdot}02\ (3)$ Å^3, $Z = 2$, $D_x = 2{\cdot}278$ Mg m^{-3}, Mo $K\alpha$, $\lambda = 0{\cdot}71069$Å, $\mu = 3{\cdot}419$ mm^{-1}, $F(000) = 254{\cdot}0$, $T = 298$ K, $R = 0{\cdot}039$ for 7667 reflections. The structural parameters are compared with those obtained by neutron diffraction. The differences between X-ray and neutron positions are related to the hydrogen bonding in the structure. The dominant features in the residual density near the two crystallographically independent Cu atoms result from the redistribution of $3d$ electrons due to bonding. The density is anisotropic, as expected in view of the Jahn-Teller distortion in the structure. Marked differences in the d-electron distributions for the two Cu atoms correlate with small variations in molecular geometry. Second-nearest-neighbour effects, such as those arising from differently oriented ligating waters, are significant in this structure. Sharp features in the difference density close to the Cu nuclei are similar to those in other Cu^{2+} complexes, indicating that the electron density in this region is more reliable than previously believed.

Introduction

Diffraction methods for the study of electron density in crystalline materials comprising first-row atoms are now well established. Charge density analyses for crystals containing heavier atoms are more difficult, in general, since the valence scattering is a lower fraction of the total for the structure. Paradoxically the case of d electrons for the heavier members of the first transition series of elements is rather favourable. Their distributions are contracted, in comparison with those for the lighter members. Because the scattering for these electrons extends correspondingly further in reciprocal space, they can be studied more accurately.

Iwata & Saito (1973) exploited this in pioneering work on hexaamminecobalt(III) hexacyanocobaltate(III). In subsequent analyses of transition-metal complexes with near-to-ideal geometry, concordance between the charge density maps and the predicted d-electron orbital occupancies was established. Lighter members of the first transition series were studied successfully by averaging regions of the electron density which, although crystallographically independent, are chemically equivalent (Rees & Mitschler, 1976). This included cases where the d electrons are involved directly in covalent bonding (Toriumi & Saito, 1978).

Qualitative information on the bonding electron distribution has already proved to be helpful in systems with non-ideal geometries, such as metal-metal bonds, where the bonding mechanism was not well understood (Wang & Coppens, 1976; Mitschler, Rees & Lehmann, 1978). In most cases, however, the nature of the stronger forces affecting the electron density distribution is well known. If charge density studies are to make a useful contribution to knowledge they

* Author to whom correspondence should be addressed.

0108-7681/85/030184-07$01.50

must explain more subtle aspects of chemical bonding, such as deviations from ideal geometry.

In this series of papers we examine charge density in non-ideal transition-metal complexes. Deviations from ideality are regarded as perturbations to the ideal geometry. Relating such perturbations to changes in density is often simpler than accounting for the total density. By the study of different types of perturbation we are able to improve our understanding of bonding as a whole.

Jahn–Teller distortions

Our starting point is the case where distorted geometry is a fundamental property of the electron configuration of the metal atom. A system in an ideal geometry with a degenerate ground state is unstable, in the sense that it has zero resistance to deformation. An infinitesimal perturbation can induce significant distortion. The case of a d^9 configuration, where the d shell has a single vacancy, is an example. Strongly distorted geometries result - as predicted by Jahn & Teller (1937).

Structures containing the Cu^{2+} ion are typical. In a study of the electron density in $KCuF_3$, Tanaka, Konishi & Marumo (1979) observed a distorted distribution. Some of the distortion can be related to differences in the lengths of the Cu–F vectors. Although other explanations have been put forward most of the remaining features can be explained in terms of the field due to the K^+ ion, but the maps also contain sharp features close to the nucleus which have not been fully explained. Tanaka & Marumo (1982) attribute these to anharmonic thermal motion. To confirm that conclusion requires an accurate neutron diffraction analysis or studies at different temperatures.

The structure of the title compound was determined by Beevers & Lipson (1934). Bacon & Curry (1962) located the protons by neutron diffraction, and Bacon & Titterton (1975) refined the structural parameters using more accurate neutron data. Supplementary structural information is now obtained by a more detailed study based on parameters derived from accurate data collected for a charge density analysis.

Experimental

Cell dimensions determined by least squares using 15 reflections with $11 < 2\theta < 37°$. Full sphere of data measured. Syntex $P\bar{1}$ diffractometer. Six standard reflections measured every 250 reflections; six scale factors evaluated with these standards consistent with mean values accurate to better than 1%. Long-term drift in beam intensity over three weeks' data collection 12%. Low-angle data measured several times. Absorption corrections evaluated by Gaussian integration, and checked by analytical evaluation using *ABSCOR* (Alcock, 1970). After correction for long-term drift, independent measurements of equivalent reflections were scrutinized for consistency with the counting statistics; outliers, in appropriate cases, were discarded. The larger of the standard deviations estimated from counting statistics or comparison of equivalents was assigned to each reflection; marked difference in these estimates occurred for the stronger reflections only. R_{int} (Table 1) evaluated after exclusion of outliers. 7667 unique reflections obtained by statistical averaging. Structure factors evaluated with the atomic scattering factors of Cromer & Mann (1968) for Cu, S and O and those of Stewart, Davidson & Simpson (1965) for H; dispersion corrections of Cromer & Liberman (1975) applied to the scattering factors of Cu and S. Structural parameters (see Table 1), the scale factor and the isotropic extinction parameter were refined to convergence with *CRYLSQ* (Stewart, 1976), using residuals based on $|F|$. Only one reflection had an extinction correction factor < 0.95.

As a check on the quality of the data, anisotropic thermal parameters for the H atoms were determined by least-squares refinement from the X-ray data. The values obtained agree with the neutron diffraction results but, having lower precision, are not recorded here. The structure is shown schematically in Fig. 1. Atomic parameters are given in Table 2,* bond lengths and angles in Fig. 2, and hydrogen-bond distances in

Table 1. *Experimental and refinement data*

Crystal dimensions

h	k	l	Distance from crystal centre (mm)
1	0	0	±0·151
1	−1	−1	±0·129
0	1	−1	±0·170

No. reflections measured	23000
No. unique reflections (N) ($0 \le h \le 13, -22 \le k \le 22, -12 \le l \le 12$)	7667
λ(Å)	0·71069
$(\sin\theta_{max})/\lambda$(Å^{-1})	1·08
Transmission range in absorption correction	0·34 to 0·54
R_{int}	0·008
w	σ^{-2}
No. parameters refined (m)†	134
Largest shift	$< 0.025\sigma$
$S^2 = \sum w\|F_o - F_c\|^2/(N-m)$	5·44
R	0·039
wR	0·025
$R(I) = \sum\|I_o - I_S\|/\sum\|I_o\|$	0·036
$\Delta\rho$ range (e Å^{-3})	−1·20 to 0·75 near Cu(2)]
Secondary-extinction parameter r^* where $F_c^* = k\|F_c\|(1 + 2r^*\|F_c\|^2\delta)^{-1/4}$ (Larson, 1970)	1·89 (2) × 10^{-5}

† Coordinates and U_{ij} for heavier atoms, coordinates only for H; U_{ij} for H set at neutron values (Bacon & Titterton, 1975).

* Lists of structure amplitudes and anisotropic thermal parameters have been deposited with the British Library Lending Division as Supplementary Publication No. SUP 39918 (22pp). Copies may be obtained through The Executive Secretary, International Union of Crystallography, 5 Abbey Square, Chester CH1 2HU, England.

Table 2. *Atomic coordinates and* U_{eq} (Å^2)

$$U_{eq}=\frac{1}{6\pi^2}\sum_i\sum_j\beta_{ij}\mathbf{a}_i.\mathbf{a}_j$$

	x	y	z	U_{eq}
Cu(1)	0·00000	0·00000	0·00000	0·0198
Cu(2)	0·50000	0·50000	0·00000	0·0260
S	0·01317 (3)	0·28636 (2)	−0·37472 (3)	0·0175
O(1)	−0·09284 (12)	0·15180 (6)	−0·32685 (12)	0·0272
O(2)	0·24421 (11)	0·31741 (7)	−0·20359 (12)	0·0187
O(3)	0·85975 (12)	0·37249 (7)	−0·36319 (12)	0·0397
O(4)	0·04314 (12)	0·30144 (7)	0·38429 (11)	0·0372
O(5)	−0·18256 (14)	0·07339 (7)	0·15133 (13)	0·0334
O(6)	0·28886 (12)	0·11724 (7)	0·14836 (13)	0·0237
O(7)	0·46547 (13)	0·40643 (8)	0·29664 (12)	0·0439
O(8)	0·75479 (14)	0·41609 (9)	0·01918 (13)	0·0625
O(9)	0·43430 (13)	0·12430 (8)	0·62801 (13)	0·0331
H(54)	−0·1146 (30)	0·1213 (18)	0·2365 (31)	
H(59)	−0·2716 (30)	0·0196 (18)	0·2070 (30)	
H(62)	0·3015 (29)	0·1876 (16)	0·0802 (29)	
H(69)	0·3241 (27)	0·1215 (15)	0·2832 (27)	
H(73)	0·5726 (27)	0·4008 (15)	0·4031 (26)	
H(74)	0·3479 (28)	0·3829 (16)	0·3269 (26)	
H(83)	0·7927 (26)	0·4020 (15)	−0·0812 (28)	
H(84)	0·8375 (28)	0·3898 (17)	0·1340 (28)	
H(91)	0·5737 (28)	0·1339 (17)	0·6521 (29)	
H(92)	0·4175 (29)	0·1852 (16)	0·6816 (30)	

Table 3. *Distances* (Å) *in hydrogen bonds*

The upper value for each distance is calculated from the X-ray coordinates in Table 2. The lower is obtained from the neutron coordinates of Bacon & Titterton (1975), with the X-ray cell dimensions.

	O···O	O–H	H···O
O(5)–H(54)···O(4)	2·848 (1)	0·739 (18)	2·138 (18)
	2·852 (4)	0·962 (6)	1·911 (6)
O(5)–H(59)···O(9)	2·765 (1)	0·812 (18)	1·963 (18)
	2·778 (4)	0·958 (5)	1·832 (6)
O(6)–H(62)···O(2)	2·794 (1)	0·808 (16)	2·040 (16)
	2·793 (4)	0·964 (8)	1·894 (6)
O(6)–H(69)···O(9)	2·739 (1)	0·774 (16)	1·967 (15)
	2·742 (4)	0·980 (4)	1·768 (4)
O(7)–H(74)···O(4)	2·758 (1)	0·775 (18)	1·988 (17)
	2·749 (3)	0·956 (4)	1·804 (4)
O(7)–H(73)···O(3)	2·711 (1)	0·772 (14)	1·946 (14)
	2·709 (3)	0·970 (3)	1·742 (3)
O(8)–H(83)···O(3)	2·670 (1)	0·747 (19)	1·926 (19)
	2·670 (4)	0·965 (6)	1·706 (6)
O(8)–H(84)···O(4)	2·705 (1)	0·780 (15)	1·934 (16)
	2·704 (3)	0·962 (4)	1·756 (4)
O(9)–H(91)···O(1)	2·779 (1)	0·808 (17)	1·976 (18)
	2·778 (3)	0·976 (4)	1·816 (4)
O(9)–H(92)···O(2)	2·992 (1)	0·802 (20)	2·226 (21)
	2·971 (6)	0·912 (12)	2·092 (10)

Table 3. Corresponding bond lengths from the neutron diffraction analysis (Bacon & Titterton, 1975) are included.

Structural geometry

Cu(1) and Cu(2) occupy the non-equivalent sites (0, 0, 0) and ($\frac{1}{2}$, $\frac{1}{2}$, 0). Both Cu atoms have four water molecules and two sulphate O atoms as ligands, arranged with approximate $4/mmm$ (D_{4h}) symmetry (Fig. 1*a*). The space-filling water differs in its relationship to the Cu atoms, as shown in Fig. 1(*b*). The elongation of the octahedron surrounding Cu(2) is larger than that for Cu(1).

Around Cu(1) the water molecules are in an approximately tetrahedral configuration defined by the two O–H vectors, by the O–Cu(1) vector, which corresponds to one of the two possible lone-pair directions, and by the other lone-pair direction. Around Cu(2) the O–Cu vectors lie close to the extension of the bisector of the angle between the O–H vectors. The geometry of the three bonds to each O (two O–H bonds and the O–Cu bond) is approximately trigonal. These trigonal waters are closer to Cu and their H–O–H angles are larger than those for the tetrahedrally oriented waters attached to Cu(1).

Bacon & Titterton (1975) have drawn attention to the H–O–H angles for the ligating waters, which may be regarded as part of a positively charged complex cation. The angles at the O atoms in the water molecules are listed in Table 4. Recently Chiari & Ferraris (1982) discussed the geometries of the water

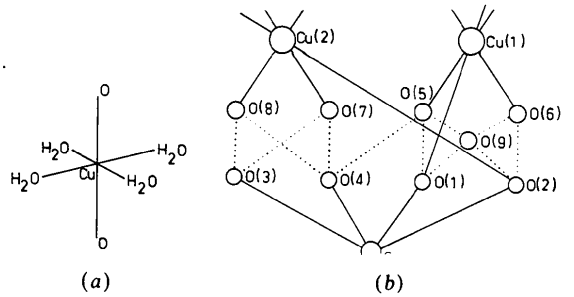

(*a*) (*b*)

Fig. 1. Schematic diagram of the bonding in the structure, showing (*a*) the Cu environment and (*b*) the hydrogen-bond network. Hydrogen bonds are dotted.

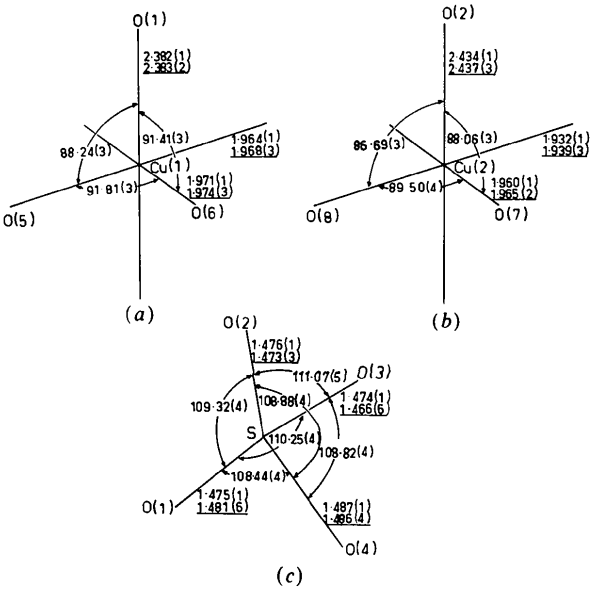

Fig. 2. Bond lengths (Å) and angles (°) involving (*a*) Cu(1), (*b*) Cu(2) and (*c*) the sulphate group. Neutron diffraction bond lengths, calculated from the coordinates of Bacon & Titterton (1975) with the X-ray cell dimensions, are underlined.

molecules, and their relationship to the environment, in a variety of hydrate structures. The H–O–H angles in these structures tend to be larger than the value for isolated water molecules. For the ligating water molecules in this structure the H–O–H angles are larger than the average values for the appropriate structure class (105·9 and 109·7° for tetrahedral and trigonal waters respectively). This is only partly accounted for by correlation with a large O···O···O angle in the hydrogen-bond network for O(5), O(6) and O(7). For O(8) this contribution should compress the H–O–H angle, according to the data of Chiari & Ferraris (1982). In fact it is enlarged.

Tentatively we regard the enlargement of the H–O–H angle, which cannot be accounted for by correlation with the O···O···O angles of the hydrogen-bond network, as an indicator of the charge on the water molecule. The $3d^9$ Cu^{2+} ion has one fewer $3d$ and one fewer $4s$ electron than the free atom. Whereas the d electron hole is close to the nucleus the $4s$ hole overlaps appreciably with the water molecules. The H–O–H angle, obtained by theoretical optimization for H_3O^+ (Lathan, Hehre, Curtiss & Pople, 1971), is approximately 10° larger than that for neutral water. In view of that result we estimate the charge on the ligating waters by linear interpolation on a scale of 10° per electron. This indicates that the water molecules O(5), O(6), O(7) and O(8) carry some tenths of an electron fewer than the space-filling water O(9). This is consistent with their forming part of a positively charged complex cation. The H–O–H angles suggest that the triangular waters, which have short Cu–O lengths, also carry higher positive charges.

Small differences in some bond lengths are associated with the number and strength of the hydrogen bonds. For example, O(8)–Cu is short, while its bonds to H(83) and H(84) are long. These two H atoms are involved in short hydrogen bonds. The O–H bonds for the space-filling water O(9) differ markedly in length, the shorter forming a weaker hydrogen bond. These properties are particular examples of quite general behaviour (Chiari & Ferraris, 1982).

The longest S–O bond involves O(4), which is the receptor for three hydrogen bonds, whereas O(1), O(2) and O(3) are receptors for two only.

X–N comparison

Comparison of X-ray and neutron positions provides information on local dipoles resulting from the redistribution of electron density, due to bonding, in the vicinity of each of the nuclei.

The X-ray and neutron coordinates of S agree within limits consistent with the e.s.d.'s. The wide range for these limits reflects the large e.s.d.'s in the neutron analysis, resulting from the low value of the scattering length for S.

Table 4. *Angles* (°) *at* O *atoms of water molecules* (*neutron values*)

	O···O···O	H–O–H
O(4),H(54)–O(5)–H(59),O(9)	120·1 (1)	108·5 (5)
O(2),H(62)–O(6)–H(69),O(9)	129·9 (2)	109·2 (6)
O(4),H(74)–O(7)–H(73),O(3)	118·3 (1)	112·9 (3)
O(3),H(83)–O(8)–H(84),O(4)	105·4 (1)	110·2 (5)
O(1),H(91)–O(9)–H(92),O(2)	122·4 (2)	107·2 (6)

The accuracy of the X-ray H positions is limited by the low scattering power of H compared with Cu and S. The existence of local dipoles, near the H nuclei, arising from a transfer of charge towards the O in O–H bonds is well known. For the O–H bonds in this structure the average value of the shortening, relative to the neutron results, is 0·179Å with r.m.s. spread of 0·033 Å. The values are largest (0·195 Å) for the triangular waters, and smallest (0·139 Å) for the space-filling water.

The difference between X-ray and neutron positions for O is smaller, but some useful information can be obtained because of the lower e.s.d.'s. X-ray and neutron positions differ primarily because of the displacement of the electron density for each O atom towards the lone pairs which are involved in hydrogen bonding. This displacement is largest [0·022 (5) Å] for the space-filling water, O(9).

For O(5), O(6), O(7) and O(8) the X-ray positions are displaced 0·005 (3), 0·007 (4), 0·005 (2) and 0·008 (2) Å respectively from the neutron positions. The corresponding reductions in Cu–O bond lengths are 0·004, 0·003, 0·005 and 0·006 Å. The bond-length shortenings and atom displacements for the triangular waters are similar because the displacement vectors are almost antiparallel to the metal–O vectors.

The S–O bond lengths in the X-ray and neutron analyses do not differ significantly because of the large uncertainty in the neutron S position. The X-ray position is more accurate, and should not be biased by bonding because of its symmetrical environment. Lengths calculated from the X-ray S and neutron O coordinates are 1·474 (3), 1·474 (2), 1·471 (3) and 1·486 (2) Å for S–O(1), S–O(2), S–O(3) and S–O(4) respectively. The X-ray values are longer by amounts which are inversely correlated with bond length. The extension is also consistent with displacement of the O atoms towards the lone-pair regions. More comprehensive information is required to establish this correlation with certainty. This point will be taken up in later papers of the series.

Difference densities

The structural parameters for first-row atoms are biased by the movement of electrons due to chemical bonding, and this has a significant effect on the residual density. Difference maps calculated with the X-ray structural parameters were featureless, except near the Cu and S atoms.

To reduce the bias, structure factors were evaluated using the first-row atom positions and the H thermal parameters from the neutron structure of Bacon & Titterton (1975). The remaining structural parameters, the scale factor for the observed structure factors, the extinction corrections and the scattering factors for the non-hydrogen atoms were taken from the X-ray structure. H scattering was evaluated using the isolated-atom form factors from *International Tables for X-ray Crystallography* (1962).

Difference density maps were evaluated for planes through the two Cu atoms containing the four water O atoms (Fig. 3*a*, *d*), and the ligating sulphate O atoms and each pair of water O atoms (Fig. 3*b*, *c*, *e*, *f*). These maps were filtered using the technique of minimum variance filtering (Davis, Maslen & Varghese, 1978). The e.s.d. in the electron density away from the nuclei is $0{\cdot}06_6$ e Å^{-3}. The corresponding maps were also evaluated using structural parameters obtained from a trial refinement with high-angle ($\sin\theta/\lambda > 0{\cdot}7$ Å^{-1}) X-ray data. They do not differ significantly from the maps shown in Fig. 3.

Whereas the Cu^{2+} ion, with a d^9 configuration, has one less $3d$ electron and one less $4s$ electron than the free atom, the difference density is based on free-atom form factors. We might expect to see evidence for the ionic state of the metal atom in the difference maps. The $4s$ density, which is rather diffuse, overlaps with the ligand atoms to which electrons have been transferred. Any subdivision of $4s$ density between the metal and the ligand atoms is rather arbitrary. The $3d$ density is closer to the nucleus. There are well defined regions of negative density around each Cu atom at a distance appropriate to the missing $3d$ electron. These regions are strongly anisotropic, with deep hollows directed towards the water O atoms.

For the Cu^{2+} ion in an ideal octahedral ligand field the $3d$ wavefunction splits into a lower triplet (t_{2g}) which is completely filled and an upper doublet (e_g) which accommodates the remaining three electrons. The state functions for the latter are $(3d_{z^2})^2\,(3d_{x^2-y^2})^1$ and $(3d_{z^2})^1(3d_{x^2-y^2})^2$. It is this degeneracy which is removed by the Jahn–Teller distortion, the four water O atoms defining the xy plane moving towards Cu, and the two sulphate O atoms along z moving away. The e_g doublet splits into two levels, d_{z^2} being stabilized and the uppermost $d_{x^2-y^2}$ being destabilized and hence only half occupied. The remaining t_{2g} orbitals

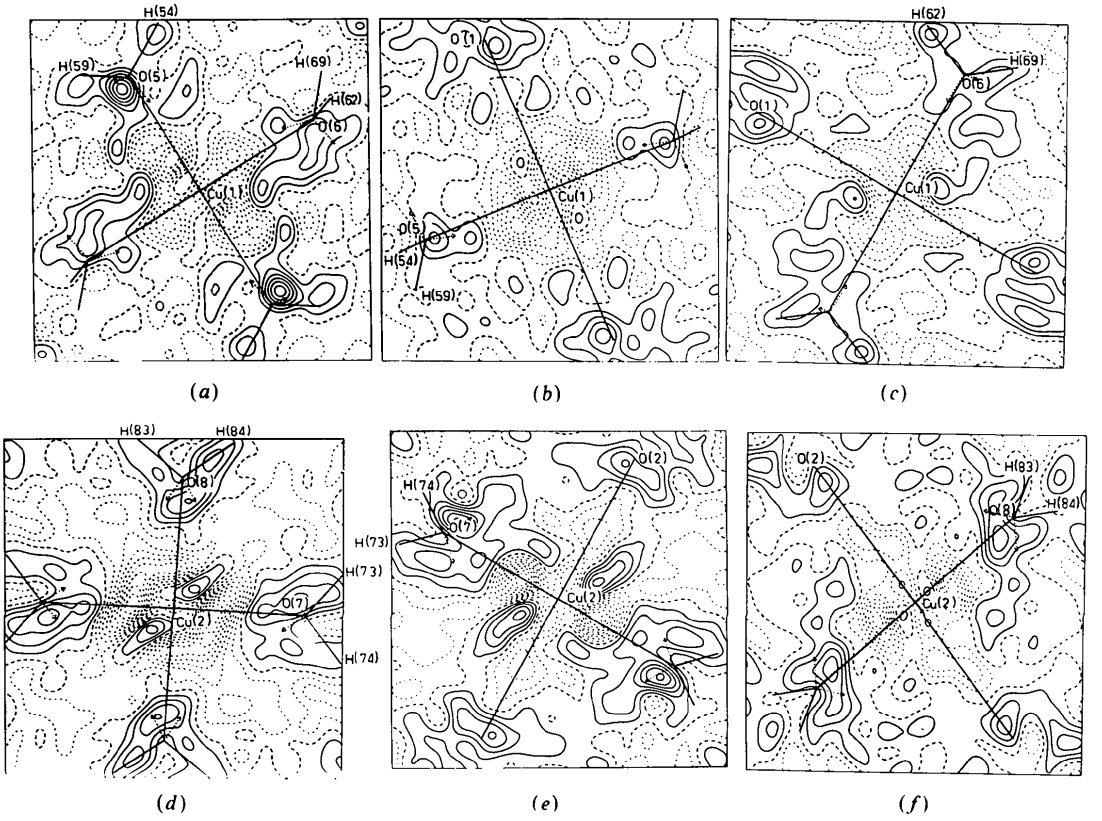

Fig. 3. Residual density for sections containing (*a*) Cu(1), O(5) and O(6), (*b*) Cu(1), O(5) and O(1), (*c*) Cu(1), O(6) and O(1), (*d*) Cu(2), O(7) and O(8), (*e*) Cu(2), O(7) and O(2), and (*f*) Cu(2), O(8) and O(2). The maps are evaluated with minimum variance filtering (Davis, Maslen & Varghese, 1978). Directions for idealized lone pairs for the water O atoms are shown by the dotted arrows. Contour interval 0·1 e Å^{-3}.

Table 5. *Integrated electron populations within a sphere of radius* 1·1 Å *centred on the* Cu *atoms*

The e.s.d.'s (in parentheses) are based on the statistical errors in the observed structure factors.

	$P_{x^2-y^2}$	P_{z^2}	P_{tot}
Cu(1)	−0·72 (1)	−0·29 (1)	−1·01 (2)
Cu(2)	−0·84 (1)	−0·12 (1)	−0·96 (2)

undergo similar splitting, but this should not affect their occupancy.

Figgis & Leckie (1981) carried out electron spin resonance experiments on copper sulphate. The anisotropy of the **g** tensor is consistent with the expected occupancies of the *d* orbitals, but the orientation of each tensor bears little relationship to the ligand geometry.

The integrated density within a distance of 1·1 Å of the Cu nuclei (the approximate distance at which the gradient of the integrated density changes sign) was evaluated for six equal parts of a sphere, described by bisecting idealized angles between the Cu–O bonds. The results are listed in Table 5. $P_{x^2-y^2}$ is the net electron count in the segments containing the Cu–O (water) vectors. P_{z^2} is the corresponding figure for the Cu–O (sulphate) vectors. P_{tot}, the total for the whole sphere, is close to the expected value of -1 in each case.

The difference densities in Fig. 3 are thus qualitatively consistent with the Jahn–Teller theorem, in so far as the hollows close to the Cu nuclei are deeper in the direction of the water ligands. However, the subdivision between $P_{x^2-y^2}$ and P_{z^2} is not as predicted by the simple arguments based on orbital occupancies.

It is possible to adjust the figures in Table 5 slightly by making reasonable changes to the volumes of integration, but the discrepancy between the two Cu atoms remains, if such changes are made in a consistent manner.

The first-order response to a modification of the potential field may be calculated by treating the electrical distribution as a classical, smeared-out charge (McWeeny & Sutcliffe, 1969). It is evident (Fig. 3) that the electron density is sensitive to small changes in the crystal field.

In each case the water O atoms which polarize the Cu atoms more strongly [O(5) and O(7) for Cu(1) and Cu(2) respectively] are involved in weaker hydrogen bonds. The deeper hollows in the difference map are close to the metal–O bonds (Fig. 3). There are peaks near the sulphate O atoms, corresponding to the lone pairs, directed towards the metal atom.

There are marked differences in the residual density for the two Cu atoms, which correlate with the molecular geometry. The electron deficiencies for the bonds linking Cu(1) to water O atoms are shallower than those near Cu(2), for which these bonds are shorter. The difference density is also less symmetric near Cu(2), which has the more distorted geometry.

There is a close relationship between the minima from the Cu–O vectors and the water O lone-pair density near Cu(1). The lone-pair directions consistent with ideal lone-pair geometry are shown by the dotted vectors in Fig. 3. For O(6), where there are weak maxima at the ideal positions, one arrow points towards the minimum near Cu. This is not true of O(5). There is, however, a strong maximum on a continuation of the H(54)–O(5) vector, approximately 0·2 Å from the ideal position, which is directed towards the minimum near Cu. The hydrogen-bond system for O(5), which has this less ideal lone-pair density, is less symmetric than that for O(6).

The effects of the electrostatic forces associated with orientations of the water molecules are particularly striking for the trigonal water molecules, which lie near the plane defined by Cu(2), O(7) and O(8). The trigonal water O(7) and O(8) are at troughs, surrounded by peaks near the O–H bonds, and along the O–Cu vector. We expect the electrostatic field due to the density to be extended in the water plane, and contracted in the direction normal to that plane. The effect of such a perturbing field is clearly evident in Fig. 3(*d*), where the hollow near O(7) is extended, and in Fig. 3(*e*), where it is contracted. O(7) has stronger peaks near the O–H bonds, and less density in the lone-pair region. The density near O(8) is qualitatively similar, but the anisotropy of the features is less pronounced.

The zeroth-order occupancies, defined as those of the 'prepared' state appropriate to the bonding configuration, are thus modified substantially by the perturbing crystal field, including effects due to the hydrogen-bond network for the ligands.

We are thus able to rationalize the difference between experiment and elementary theory based on atomic state occupancies. The latter is too simplistic to account for all the features in the electron density shown by the diffraction experiment. But what of the apparent conflict between the diffraction result, which gives non-integral populations for orbitals aligned quite close to the molecular axes, and the ESR experiment, which is consistent with integral populations, but requires principal axes oblique to the molecular axes?

When the **g** tensors of Figgis & Leckie (1981) for the Cu atoms were superimposed on the difference density it was found that there was close correspondence between those principal axes and those of the density close to the nuclei! These deviate substantially from the molecular axes which are such a good fit to the main part of the *d*-electron density.

It is generally considered that, because of uncertainty in the scale factor, the appearance of a difference density map near an atomic nucleus is unreliable. A small change in the scale factor will have a dramatic

effect on the difference density, yet we have close correspondence between the **g** tensor orientation from the ESR experiment and this allegedly unreliable density. The point to be noted is that the uncertainty in the scale factor affects a contribution to the density with the form of an image of the whole atom. This is an almost spherical, or scalar, component since the thermal motions for the Cu atoms are close to isotropic. The orientation of the difference density near the Cu nuclei is determined by higher-order Fourier components, which are largely independent of the error in the scale factor. Thus the correspondence between orientations of the **g** tensor and the difference density is not unreasonable.

The difference maps in Fig. 3 were calculated by the minimum variance filtering method (Davis *et al.*, 1978). We obtain higher resolution, at the penalty of increased uncertainty, in unfiltered maps. Fig. 4 shows an unfiltered equivalent of Fig. 3(*f*). The density near the Cu nucleus has a remarkable resemblance to the corresponding region of the difference map for $KCuF_3$ shown in their Fig. 2(*b*) by Tanaka *et al.* (1979). Closely similar features are observed for other Cu^{2+} complexes, which will be described in later papers in this series. The similarity implies that, provided the scalar term (or more accurately an image of the total density) can be discounted, the difference density near the nucleus contains useful information.

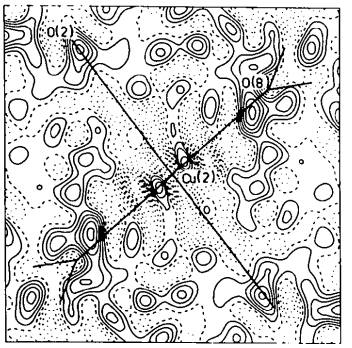

Fig. 4. Residual density for the section containing Cu(2), O(2) and O(8). Contour interval 0·1 e $Å^{-3}$. Unfiltered map.

All calculations were performed on a Perkin-Elmer 3241 computer using programs from the *XRAY*76 system (Stewart, 1976). This work has been supported financially by the Australian Research Grants Committee, by the Australian Institute of Nuclear Science and Engineering and by the University of Western Australia Research Committee. We also thank Dr A. H. White who collected three sets of X-ray data.

References

ALCOCK, N. W. (1970). *Crystallographic Computing*, edited by F. R. AHMED, pp. 271-278. Copenhagen: Munksgaard.

BACON, G. E. & CURRY, N. A. (1962). *Proc. R. Soc. London Ser. A*, **266**, 95-108.

BACON, G. E. & TITTERTON, D. H. (1975). *Z. Kristallogr.* **141**, 330-341.

BEEVERS, C. H. & LIPSON, H. (1934). *Proc. R. Soc. London Ser. A*, **146**, 570-582.

CHIARI, G. & FERRARIS, G. (1982). *Acta Cryst.* B**38**, 2331-2341.

CROMER, D. T. & LIBERMAN, D. (1970). *J. Chem. Phys.* **53**, 1891-1898.

CROMER, D. T. & MANN, J. B. (1968). *Acta Cryst.* A**24**, 321-324.

DAVIS, C. L., MASLEN, E. N. & VARGHESE, J. N. (1978). *Acta Cryst.* A**34**, 371-377.

FIGGIS, B. N. & LECKIE, R. (1981). *Aust. J. Chem.* **34**, 2019-2023.

International Tables for X-ray Crystallography (1962). Vol. III. Birmingham: Kynoch Press. (Present distributor D. Reidel, Dordrecht.)

IWATA, M. & SAITO, Y. (1973). *Acta Cryst.* B**29**, 822-832.

JAHN, H. A. & TELLER, E. (1937). *Proc. R. Soc. London Ser. A*, **161**, 220-235.

LARSON, A. C. (1970). *Crystallographic Computing*, edited by F. R. AHMED, pp. 209-213. Copenhagen: Munksgaard.

LATHAN, W. A., HEHRE, W. J., CURTISS, L. A. & POPLE J. A. (1971). *J. Am. Chem. Soc.* **93**, 6377-6387.

MCWEENY, R. & SUTCLIFFE, B. T. (1969). *Theoretical Chemistry.* Vol. 2. *Methods of Molecular Quantum Mechanics*, edited by D. P. CRAIG & R. MCWEENY, pp. 96-98. London: Academic Press.

MITSCHLER, A., REES, B. & LEHMANN, M. S. (1978). *J. Am. Chem. Soc.* **100**, 3390-3397.

REES, B. & MITSCHLER, A. (1976). *J. Am. Chem. Soc.* **98**, 7918-7924.

STEWART, J. M. (1976). The *XRAY*76 system. Tech. Rep. TR-446. Computer Science Center, Univ. of Maryland, College Park, Maryland.

STEWART, R. F., DAVIDSON, E. R. & SIMPSON, W. T. (1965). *J. Chem. Phys.* **42**, 3175-3187.

TANAKA, K., KONISHI, M. & MARUMO, F. (1979). *Acta Cryst.* B**35**, 1303-1308.

TANAKA, K. & MARUMO, F. (1982). *Acta Cryst.* B**38**, 1422-1427.

TORIUMI, K. & SAITO, Y. (1978). *Acta Cryst.* B**34**, 3149-3156.

WANG, Y. & COPPENS, P. (1976). *Inorg. Chem.* **15**, 1122-1127.